Hydrogen Isotope Labeling of Pharmaceuticals via Dual Hydrogen Isotope Exchange Pathways

Rajendra Maity,[1,2] Otto Dungan,[3] Frédéric A. Perras,[4,5] Jingwei Li,[3]* Daohua Liu,[1] Sumei Ren,[3] Dan Lehnherr,[3] Zheng Huang,[3] Eric M. Phillips,[3] Moses Adeyemo,[1] Joseph Frimpong,[1] Timothy Quainoo,[1] Zhen-Fei Liu,[1] and Long Luo[1,2] *

Affiliations:

[1]Department of Chemistry, Wayne State University, 5101 Cass Avenue, Detroit, MI 48202, United States.

[2]Department of Chemistry, University of Utah, 315 S 1400 E, Salt Lake City, UT 84112, United States.

[3]Process Research and Development, Merck & Co., Inc., Rahway, NJ 07065, United States.

[4]Chemical and Biological Sciences Division, Ames National Laboratory, Ames, Iowa 50011, United States

[5]Department of Chemistry, Iowa State University, Ames, Iowa 50011, United States

*Corresponding authors: jingwei.li1@merck.com, long.luo@utah.edu

Abstract: Isotopic labeling is a powerful technique extensively used in the pharmaceutical industry. By tracking isotope-labeled molecules, researchers gain unique and invaluable insights into the pharmacokinetics and pharmacodynamics of new drug candidates. Hydrogen isotope labeling is particularly important as hydrogen is ubiquitous in organic molecules in biological systems, and it can be introduced effectively through late-stage hydrogen isotope exchange (HIE). However, most of the current methods require directing groups, which leaves a gap for simultaneously labeling multiple sites with varying types of C-H bonds in the molecules. Herein, we demonstrate a heterogeneous photocatalytic system that proceeds via a unique dual HIE pathway mechanism—one occurs in the reaction solution and the other on the catalytic surface—to address it. This protocol has been successfully applied to the high incorporation of deuterium and tritium in 26 commercially available drugs.

One-Sentence Summary: A method that combines surface and solution pathways achieves the maximum hydrogen labeling efficiency.

Introduction

Isotopic labeling is a powerful technique extensively used in the pharmaceutical industry. (*1-4*) This technique involves incorporating either stable isotopes, such as deuterium (D) and carbon-13 (^{13}C), or radioactive isotopes, such as tritium (T), into molecules. By tracking these labeled molecules, researchers gain invaluable insights into the pharmacokinetics and pharmacodynamics of new drug candidates. Such information is critical to understanding how drugs are absorbed, distributed, metabolized, and excreted (ADME studies) in living organisms. Hydrogen isotope labeling is particularly important as hydrogen is present in all organic molecules in biological systems. (*5, 6*) Most recently, there has also been pronounced interest in developing deuterated drugs in which D incorporation may improve the pharmacokinetics, leading to enhancement of efficacy and safety. (*7*) Deutetrabenazine for treating chorea associated with Huntington's disease became the first deuterated drug to receive U.S. Food and Drug Administration approval in 2017. (*8*)

Requirements of hydrogen isotope labeling vary by their targeted applications (**Fig. 1a**). For example, when deuterated compounds are used as an internal standard for the mass spectrometry analysis of small molecules, the mass increase for the labeled compounds should be larger than 3 Ds per molecule (≥ 5D atoms if one Cl or Br atom is present) to ensure proper resolution from the mass signals of an unlabeled analyte. (9) Low-specific activity T-labeled compounds that are labeled at a metabolically stable position are often needed for metabolism studies to support the ADME profiling of pharmaceuticals. (10) Meanwhile, a high specific activity is often required to study specific pharmacological interactions between a radiolabeled ligand and its target (11) and in autoradiography imaging. (12)

Hydrogen isotope exchange (HIE) is the most attractive approach to D/T-labeling as it allows rapid and direct isotope incorporation into pharmaceuticals at a late stage. Current HIE strategies include (i) homogenous catalysis using transition metal complexes such as [Ir], (*9, 10*) [Co], (*11*) [Ni], (*12*) and [Fe], (*13*) and alkali metal amides; (*14, 15*) (ii) photoredox catalysis using molecular photocatalysts such as [Ir], Cz-IPN (*16-18*) and decatungstate (*19*) coupled with a hydrogen atom transfer (HAT) catalyst such as thiol or transition metal hydride, (iii) heterogeneous catalysis using metal particles such as Ru, (*20, 21*) Rh, (*22*) Ir, (*10*) and Pt, (*23*) and most recently, (iv) electrochemical methods that generate radical or ionic intermediates for D incorporation. (*24-26*)

Fig. 1b lists each HIE strategy's main advantages and limitations. First, homogenous catalysis methods typically install D/T at specific aromatic C(sp^2)–H sites next to a directing group. (*14, 27*) Next, photoredox catalysis methods mainly incorporate D/T at α-amino and formyl C–H bonds of drug molecules. (*16, 17, 19, 28*) In comparison, heterogeneous catalysis methods using metal particles could label different types of sites. The shortcomings of current heterogeneous catalysis are (i) when multiple sites are present in a molecule, the competition for the catalyst surface binding sites limits the overall labeling efficiency, and (ii) the use of high concentrations of radioactive tritium gas to achieve high T incorporation. (*20, 22*) Electrochemical HIE methods are in their infancy and have only been demonstrated on simple amines and pyridines. (*24, 25*) Overall, all these methods are mostly restricted to targeting one specific type of site. HIE methods that consistently and simultaneously label multiple sites with different C–H bond types are still lacking.

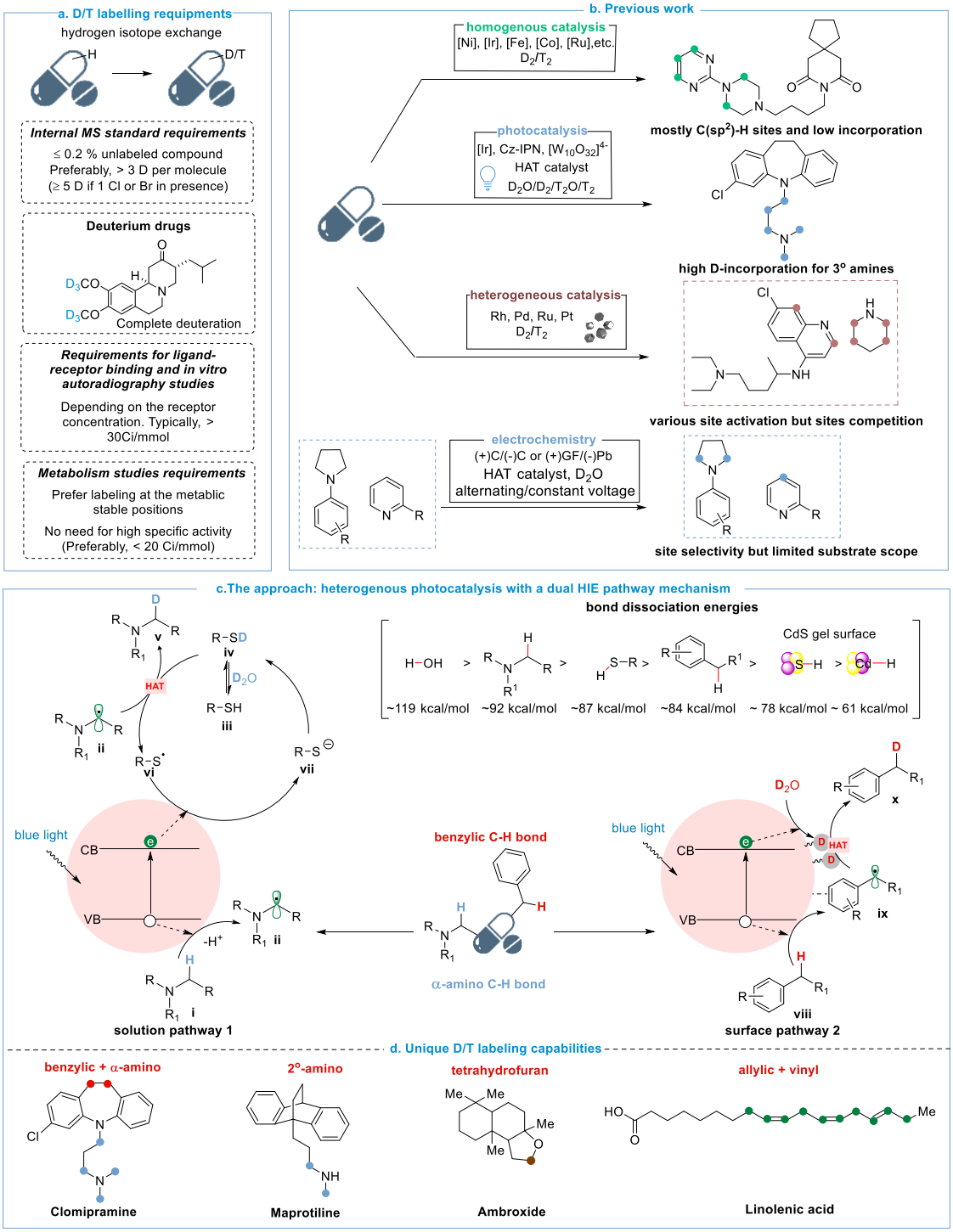

Fig. 1. Background and proposed HIE method. (a) General D/T labeling requirements for various applications in the pharmaceutical industry. (b) Existing HIE methods. (c) Proposed heterogeneous photocatalytic HIE method using a CdS QD gel catalyst that proceeds via a dual HIE pathway mechanism. (d) Unique hydrogen isotope labeling capabilities of our method, including multiple site labeling, labeling α-C–H bonds of secondary amines and ethers, and allyl and vinyl sites.

Method design and reaction development

Here, we designed a heterogeneous photocatalytic HIE method to address the unmet needs for multiple-site labeling of pharmaceuticals (**Fig. 1c**). In our design, we used CdS quantum dot (QD) gels—a 3-dimensional mesoporous network of CdS QDs with most surface ligands removed (**Fig. S1-S2**) (*29-31*)—as the photocatalyst. Metal chalcogenide QDs, including CdS and CdSe, are a group of emerging photocatalysts that enable unique organic transformations such as direct photocatalytic hydrogen atom abstraction, (*32*) radical-radical cross-coupling, (*33*) and regioselective [2+2] cyclic addition. (*34, 35*) We hypothesized that this CdS photocatalytic system could provide two parallel HIE pathways for simultaneously labeling different sites: one in solution and the other on the catalyst surface.

In solution, the CdS catalyst generates radical intermediates via single electron transfer events upon photoexcitation. The formed radicals react with a solution-phase HAT catalyst, such as a deuterated thiol, to be deuterated. (*17*) However, because the S−H bond dissociation energy (BDE) of thiols (≈ 87.0 kcal/mol) is relatively large, thiols cannot efficiently transfer D/T atoms to C–H bonds with low BDEs such as benzylic C−H bonds (≈74 to 88 kcal/mol). (*36*) This limitation can be overcome via the surface pathway, in which the CdS catalyst surface stabilizes D atoms with low calculated BDEs of ≈61 to 78 kcal/mol (**Fig. S4**), mediating the transfer of D atoms to the surface-bound radical intermediates. The two independent pathways enable the simultaneous labeling of pharmaceuticals at different types of sites, such as benzylic and α-amino sites, while minimizing the competition for catalytic surface sites (**Fig. 1d**). In addition, Cd chalcogenide surfaces are known to stabilize secondary amines, (*37*) activate cyclic ethers, (*32*) and stabilize allylic and vinylic radicals, (*17, 33, 38*) facilitating their HIE reactions.

We initiated our studies using a commercial antidepressant, clomipramine (**1**), which contains both an alkyl amine moiety and benzylic sites, as a model substrate. We used triisopropylsilanthiol as the solution-phase HAT catalyst and D_2O as a D source (**Fig. 2**). The results show that the CdS photocatalyst delivered the deuterated product **[^{2}H]1** with an impressive 11.7 D/molecule with less than < 0.1% of the unlabeled compound remaining (**Fig. S9**). The two benzylic and four α-amino sites were highly deuterated to levels of 76% and 74-86%, respectively (**Fig. 2**). In comparison, existing photoredox protocols using molecular photocatalysts primarily activate the α-amino C−H bonds, giving a total of 6 to 7 D/molecule (**Fig. S11**). (*17*) Despite varying the solvent, thiol type, light intensity, reaction time, D_2O equivalent, and base addition, effective D incorporation at both sites remained unchanged (**Table S1-S6**). Comparable results were obtained with a scale-up reaction or a recovered CdS photocatalyst (**Fig. S12**). The light on/off experiment showed that D-labeling increased only when the light was on, indicating that the HIE reaction is a light-driven process (**Fig. S13**). A radical capture experiment using methyl vinyl ketone as the radical acceptor showed the formation of tri-alkylated products of **1** (**Fig. S14**), suggesting that the radical centers are generated under HIE reaction conditions, possibly at various sites of **1**.

The optimal protocol was applied to 26 commercially available drugs. We first tested drug molecules consisting of benzylic and tertiary alkyl amine scaffolds (**2-6**). Efficient D incorporation at both types of sites was obtained, similar to **1** (**Fig. 2**). For example, aripiprazole (**3**) accomplished 61% deuteration at its benzylic position in a lactam ring (3-fold higher than the existing method, **Fig. S11**) and 46%-89% deuteration at its piperazine α-amino sites. High labeling efficiency was also achieved at acyclic benzylic positions of cloperastine (**4**, 97%), carbinoxamine (**5**, 32%), and pimozide (**6**, 50%) while achieving high labeling efficiencies of 50% to 90% at their α-amino positions. In certain cases, β-amino positions were also deuterated (e.g., 46% for **6**).

Without alkyl amine moieties, the HIE at benzylic positions remained efficient, with a D incorporation of ~70% for pyroquilon (**7**) and pioglitazone (**8**). The α-position adjacent to the carbonyl carbon of **8** also completely exchanged with D. Drug molecules with only tertiary alkyl

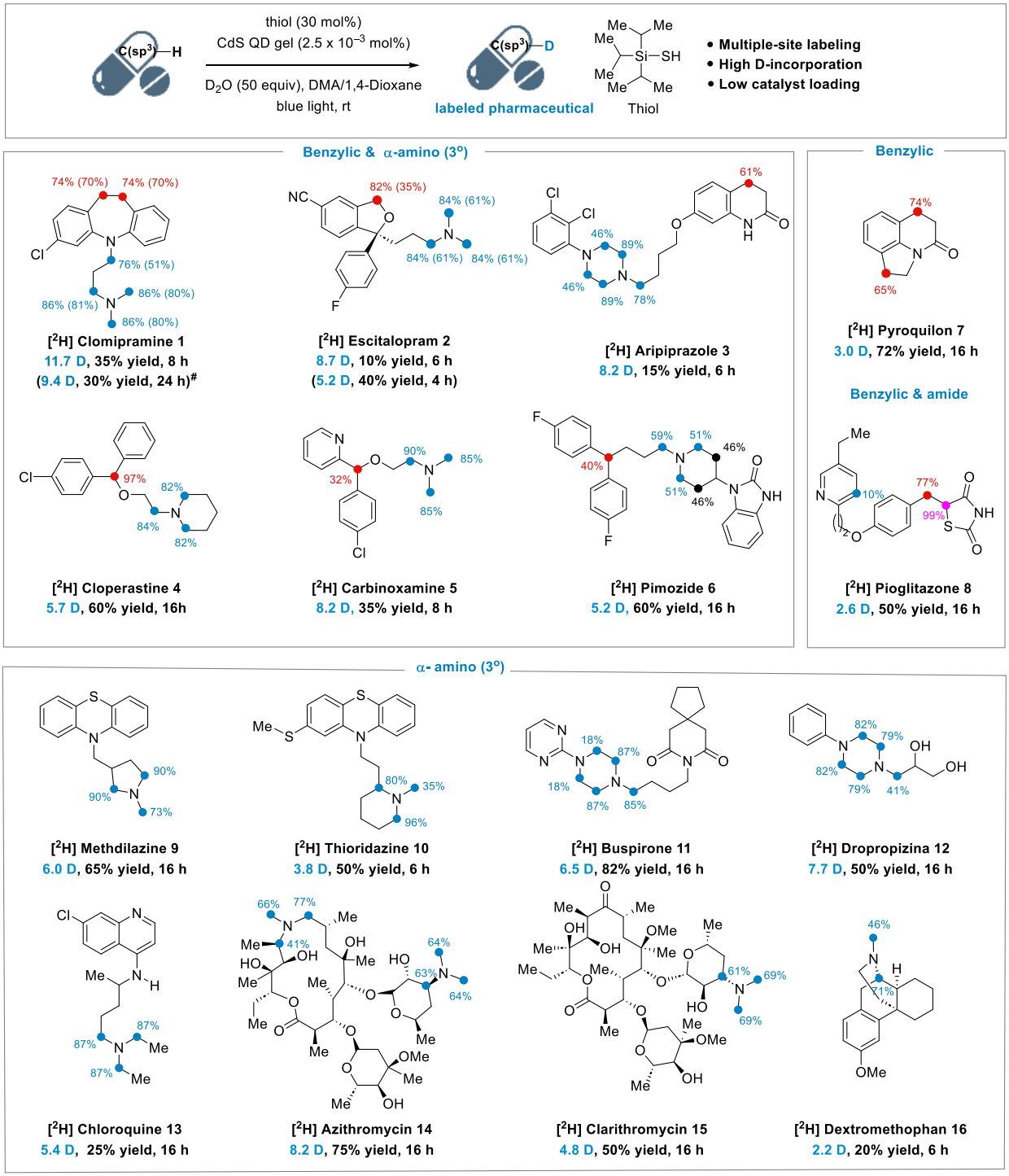

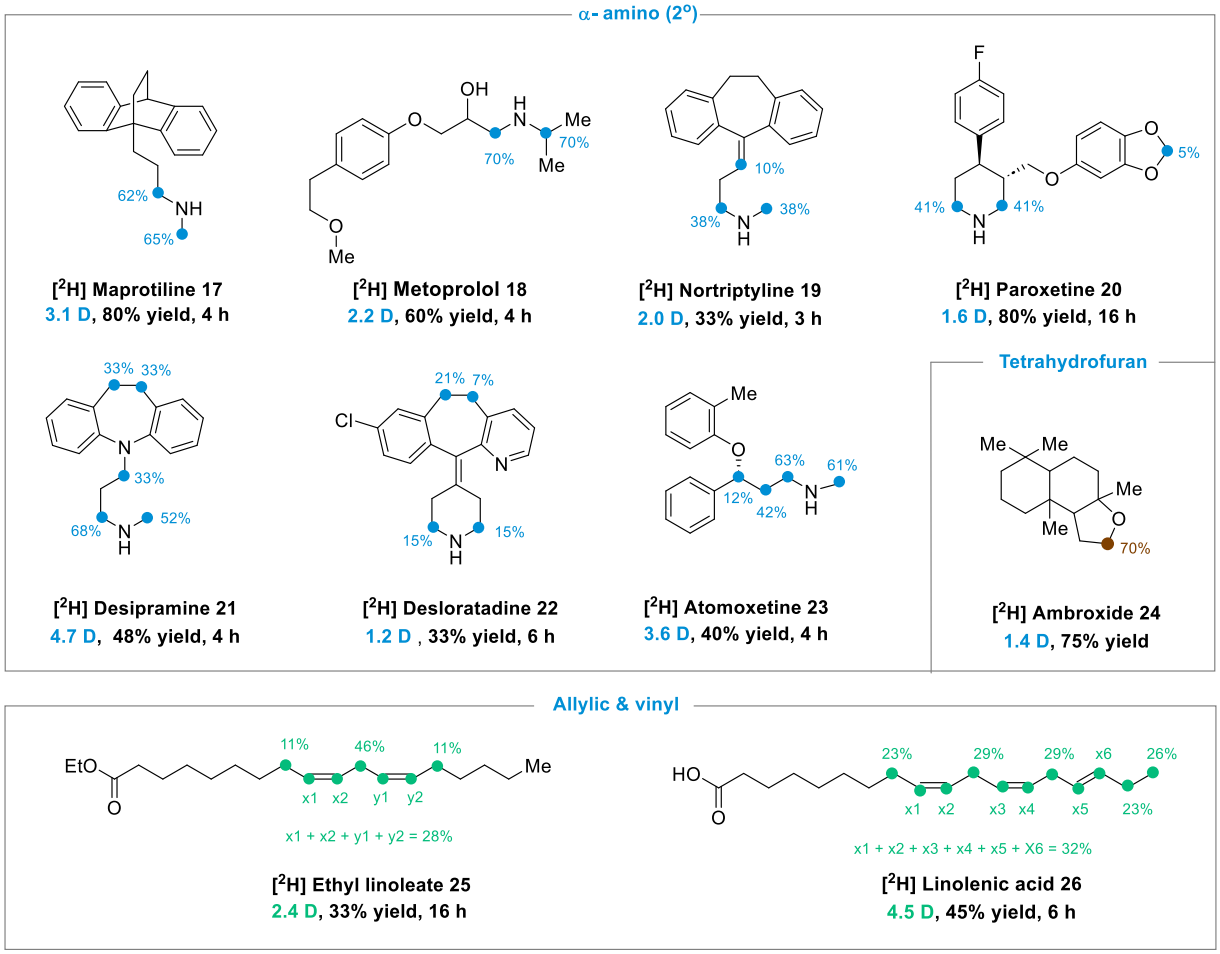

Fig. 2. Scope for the H/D exchange of pharmaceuticals. Reaction conditions: substrate (0.2 mmol, 1.0 equiv), DMA or dioxane (2 mL, 0.1 M), triisopropylsilanethiol (0.06 mmol, 0.3 equiv), D_2O (10 mmol, 50 equiv) and CdS gel (125 μL, 2.5×10^{-3} mol%); $^{\#}$2 mmol scale reaction data for substrate **1**.

amine scaffolds also showed high D-incorporation at their α-amino sites, producing **[^{2}H]9**-methdilazine (6.0 D/molecule), **[^{2}H]10**-thioridazine (3.8 D/molecule), **[^{2}H]11**-buspirone (6.5 D/molecule), **[^{2}H]12**-dropropizine (7.7 D/molecule) and **[^{2}H]13**-chloroquine (5.4 D/molecule). Macrocyclic drugs, such as **[^{2}H]15**-azithromycin and **[^{2}H]16**-clarithromycin, delivered D-incorporation values of 8.3 D and 4.8 D, respectively. In the case of dextromethorphan (**16**), only its α-amino positions were deuterated, possibly because its T-shaped configuration caused steric hindrance for the interaction between the benzylic C−H bond and the CdS surface.

Next, we expanded the substrate scope to drugs with secondary amine and benzylic scaffolds. Directly labeling secondary amines is challenging because homogenous metal catalysts often coordinate with them, preventing the delivery of HIE products. (*39, 40*) There are only limited reported methods for secondary amine deuteration with scattered examples. (*22, 41, 42*) Our method smoothly labeled the α-position of secondary amines with a D incorporation of 40% to 70% and a good yield of 33% to 80% (**[^{2}H]17** to **[^{2}H]23**). Benzylic site labeling was, however, suppressed for these substrates, possibly because the secondary amine sites outcompeted benzylic sites for CdS surface sites, blocking the surface pathway for benzylic site labeling. During the HIE

reactions, a wide range of functional groups such as alcohol, halogen (F and Cl), cyano, allyl, amide, carbonyl, pyridine, and thio/ether groups were well tolerated, and the stereogenic centers were retained (**Fig. S15** and **S16**).

Labeling the α-C−H bonds of cyclic ethers, such as ambroxide (**24**, 1.4 D/molecule), and allylic and vinyl C−H bonds of poly-alkenes, such as ethyl linoleate (**25**, 2.4 D/molecule) and linolenic acid (**26**, 4.5 D/molecule) were also successful. Poly-alkene deuteration is difficult because of possible double bond migration and hydrogenation under the HIE conditions. The H/D exchange results above clearly demonstrated the versatility of our heterogeneous photocatalytic HIE method for labeling various C-H bonds.

Further optimization was performed for tritiation (**Tables S9-13).** Successful tritiations were achieved after slightly tuning the reaction parameters (**Fig. 3**). Cloperastine (**4**) was successfully labeled under 2 h irradiation to give 88 mCi of product at 75 Ci/mmol, doubling the T incorporation by the previously reported method (**Fig. S11**). (*17*) Not surprisingly, T labeling was achieved on both benzylic (41%) and α-amine C(sp^3)−H sites (33% and 38%), consistent with the deuteration results. Other substrates were also efficiently labeled with this method: **1** (46 Ci/mmol), **6** (41 Ci/mmol), **11** (52 Ci/mmol), and **15** (72 Ci/mmol). For **1** and **6**, the limited T incorporation at the benzylic site could be attributed to the reduced reaction time in tritiation to prevent decomposition. Despite the significant advancements in HIE method development in recent years, certain functional groups, such as secondary amines, are still not amenable to generating high-specific activity T tracers. (*43-45*) With this QD-catalyzed HIE method, we successfully labeled a secondary amine, **17**, at the α-position with high specific activity (56 Ci/mmol).

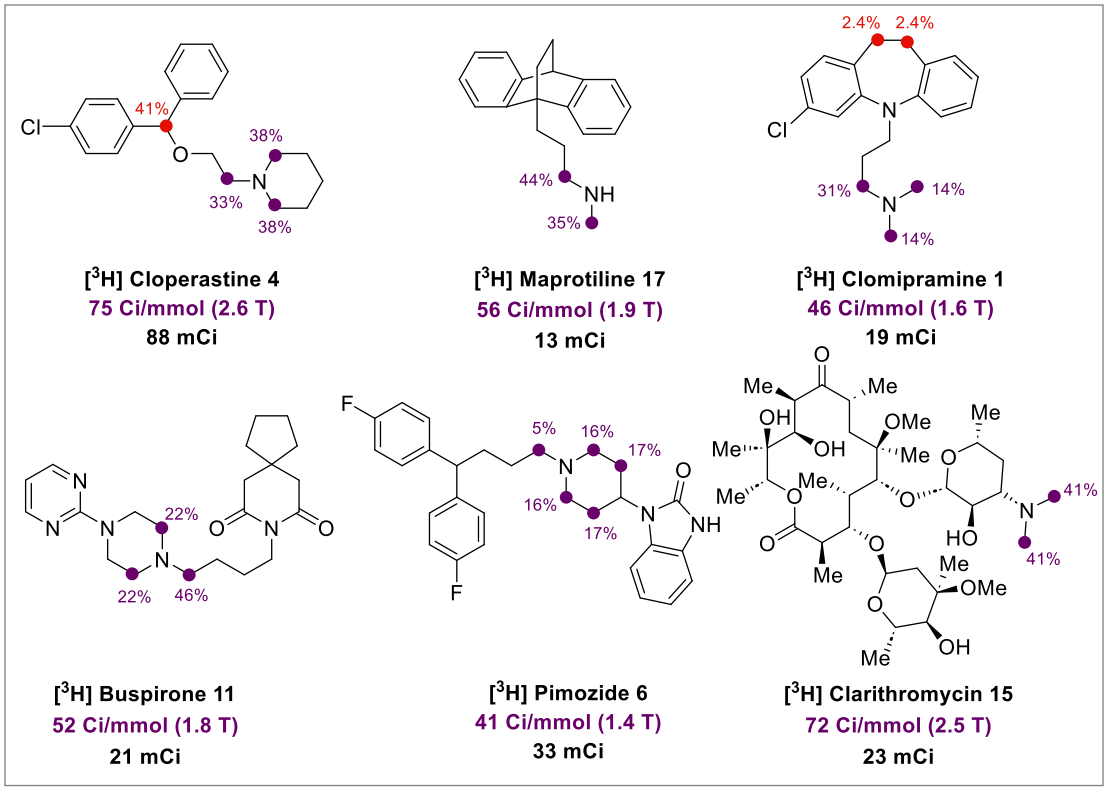

Fig. 3. Scope for the H/T exchange of pharmaceuticals. Reaction conditions: substrate (1 µmol), CdS gel photocatalyst (10 µL, 40 × 10^{-3} mol%), thiol catalyst (triisopropylsilanethiol, 30 mol%). T_2O (generated from 2 Ci of T_2 and PtO_2). The reaction was irradiated in the integrated photoreactor at 65% intensity.

Mechanistic studies

We performed a series of mechanistic experiments to gain comprehensive insights into the HIE mechanism. First, we confirmed that the HIE reactions at the benzylic and tertiary α-amino C−H sites occurred simultaneously, rather than sequentially, by monitoring the D incorporation evolution at each site of **1** (**Fig. 4a** and **Table S5**).

Next, we identified that the HIE at the benzylic and tertiary α-amino C−H sites proceeded via two independent pathways. As illustrated in **Fig. 4b**, our proposed HIE reaction undergoes a dual HIE pathway mechanism, in which thiol is the HAT catalyst for the solution pathway, and CdS surface is the HAT catalyst for the surface pathway. Without thiol, the solution pathway would be shut down, whereas the surface pathway would not. **Fig. 4c** compares the HIE results for **1** with and without thiol. We found that removing thiol inhibited the HIE at its α-amino sites with D incorporation of 2 to 8%, whereas its benzylic C−H sites still showed moderate D incorporation of ~38%. With the thiol loading gradually increased from 0 to 30 mol%, the D incorporation gradually increased to 74% for the benzylic C-H bonds, whereas it soared from 4% to 86% for α-amino C−H bonds (**Table S7**). Similar D labeling differences were observed for **2** and **4** (**Fig. 4c**). When only benzylic sites are present, like in **7**, its D incorporation was successful without thiol. In contrast, the absence of thiol failed to incorporate any deuterons into **11**, which has only tertiary α-amino sites. These findings indicate that the HIE at tertiary α-amino sites almost exclusively proceeded via the solution pathway that required thiol as the HAT catalyst, whereas the HIE at the benzylic site primarily proceeded via the surface pathway.

We further used trioctylphosphine oxide ligand-capped CdS QDs as a negative control to block the surface pathway. We observed that the D incorporation at benzylic sites of **1** was low (only 11%), whereas its α-amino sites were less affected (29% to 83%) under the optimal HIE conditions (**Table S8**). Without thiol, both types of sites became silent (**Table S7**). This observation further supports our assignments on the two HIE pathways. In addition, we also tested commercially available CdS powder. We observed a similar D labeling pattern as QD gels with and without thiol (**Table S7** and **S8**), indicating the unique HIE reactivity is inherent to different CdS materials.

During the substrate scope development, we found that the presence of secondary amine moieties suppressed the benzylic site labeling. We attributed it to secondary amines outcompeting benzylic sites over the CdS surface sites. To test this hypothesis, we carried out the HIE reaction without thiol for **17** and **21**. Interestingly, the absence of thiol did not turn off the D incorporation at secondary α-amino positions (**Fig. 4c**), supporting the proposed explanation. In the case of conjugated poly-alkenes such as **25**, only the allyl site between the alkenes was labeled in the absence of thiol. This result suggests that these substrates interact with the CdS surface via their alkene moiety during the HIE reaction.

As alluded to above, the D labeling through the surface pathway is determined by how a drug molecule interacts with the CdS catalyst surface. To decipher the above D-labeling results, we computed the binding conformations of drug molecules on a CdS QD surface. **Fig. 4d** shows the size comparison between **1** and one CdS QD in the gel catalyst. We varied the molecule orientation on the CdS surface and calculated the binding energies of different conformations (**Fig. S5**). **Fig. 4f** shows one stable binding confirmation of **1** on the CdS surface. From the different conformations results, we deduced each moiety's contributions in **1** to the total binding energy (**Fig. S5**). **Fig. 4e** shows the two phenyl rings are the strongest binding moieties with a binding energy contribution of 46 kcal/mol, suggesting that **1** preferentially binds to the CdS surface through the phenyl rings.

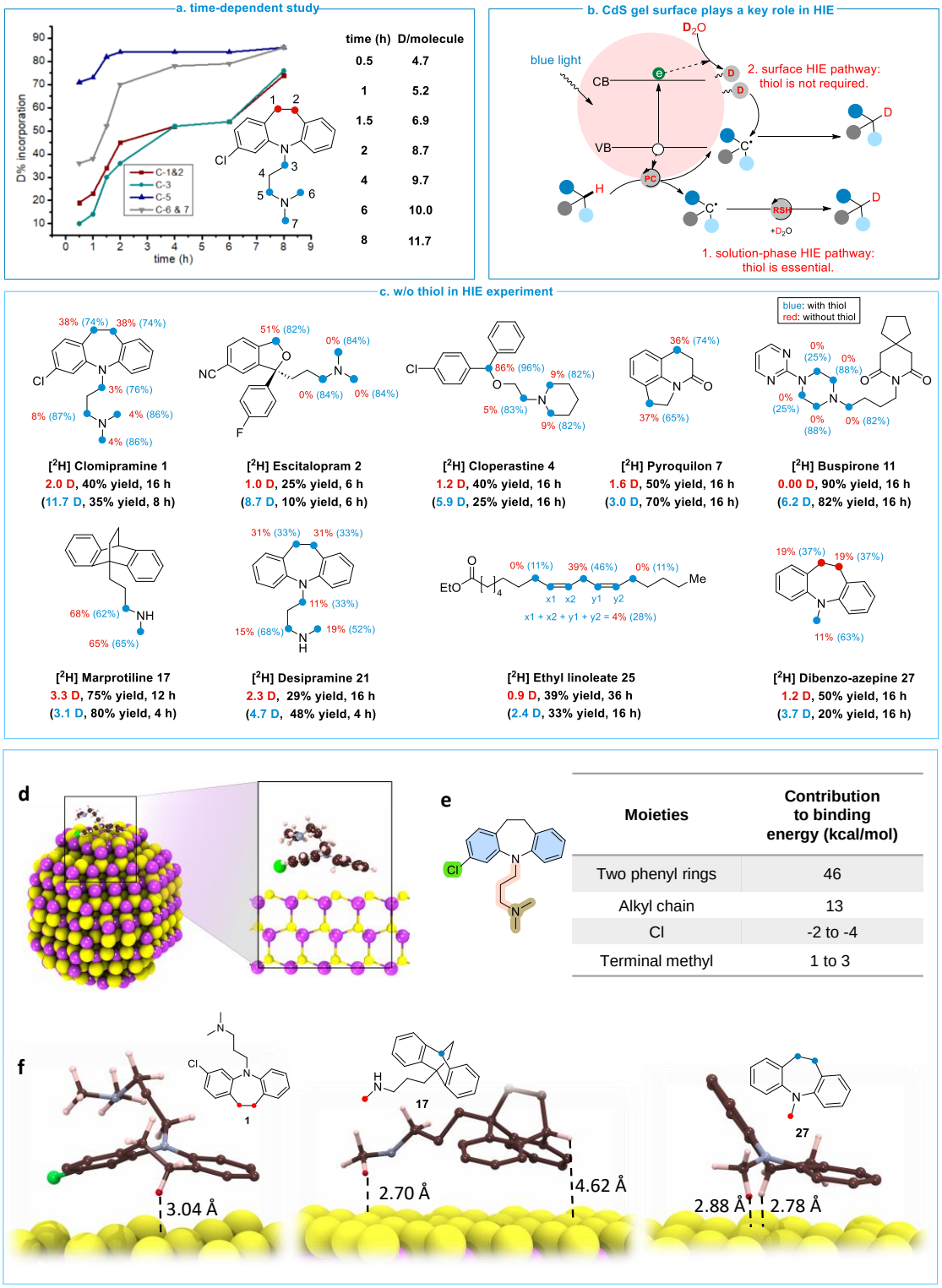

Moieties	Contribution to binding energy (kcal/mol)
Two phenyl rings	46
Alkyl chain	13
Cl	-2 to -4
Terminal methyl	1 to 3

Fig. 4. Mechanistic studies. (a) %D incorporation at different sites as a function of reaction time. (b) Proposed dual HIE pathway mechanism. (c) HIE experiment results with and without thiol catalyst. Reaction conditions: substrate (0.2 mmol, 1.0 equiv), DMA or dioxane (2 mL, 0.1 M), D_2O (10 mmol, 50 equiv) and CdS gel (125 μL, 2.5×10^{-3} mol%). (d) Size comparison between a CdS QD and **1**. (e) Binding energy contribution of different moieties of **1**. (f) Stable binding conformation of **1**, **17,** and **27** on a CdS surface.

Similar simulations were conducted for **17**. In its strongest binding conformation, the amine moiety is bound to the CdS surface (**Fig. 4e** and **S8**). However, due to its bicyclic structure, the distance between the benzylic C–H and CdS surface is ~4.62 Å, which is prohibitive for the HAT process (typically, the HAT distance should be ≤ 3 Å). (*46*) This finding is consistent with the experimental result of no D-labeling at the benzylic site of **17** (**Fig. 4c**). In addition, we studied dibenzo-azepine (**27**), which has a similar structure as **1** but replaces the alkyl amine chain of **1** with a methyl group. The C−H bonds on the methyl group of **27** are free to rotate. They thus could have a similar distance of ~2.8 Å to the CdS surface as benzylic C−H bonds (**Fig. 4f**). We observed comparable D-labeling at both sites (11% vs. 19%) in the absence of thiol (**Fig. 4c**). These results indicate that the distance between the H atom to be exchanged and the CdS catalytic surface dictates the D labeling efficiency via the surface pathway.

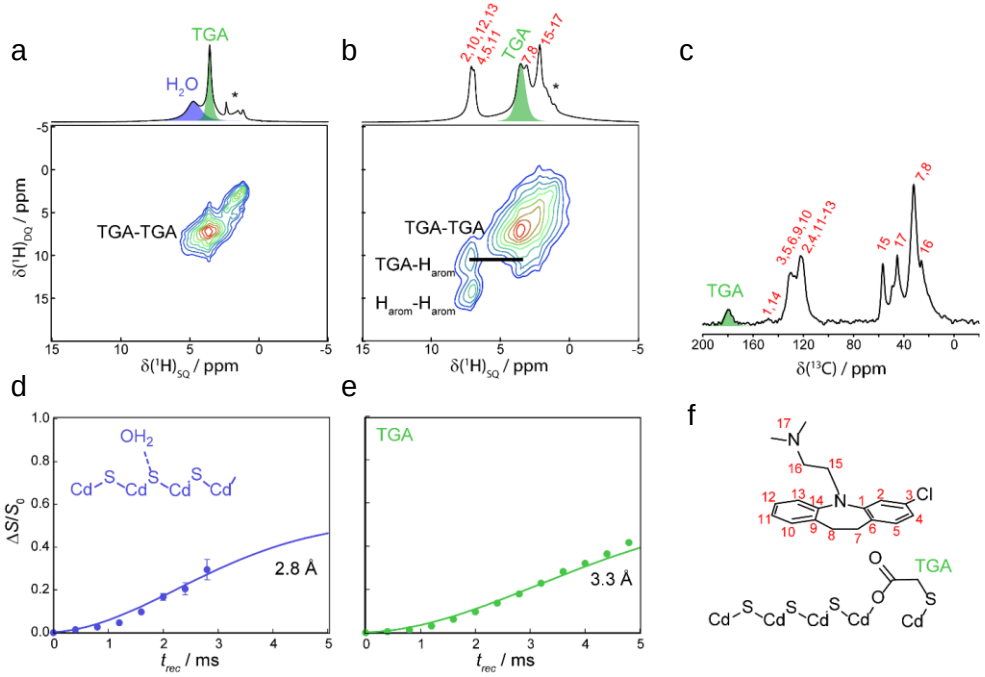

Fig. 5. Solid-state NMR studies. ^{1}H 1D fast-MAS and 2D DQ/SQ correlation spectra acquired for (a) bare CdS gel and (b) one washed with a CH_2Cl_2 solution of **1**. (c) ^{13}C CPMAS NMR spectrum of the latter material. ^{1}H–^{111}Cd DE-S-REDOR dephasing curves and fits for the signals resonating at (d) 4.7 ppm and (e) 3.6 ppm assigned to physiosorbed water and thioglycolate, respectively. (f) A model of surface adsorption of **1** agrees with the observed correlations between ^{1}H–^{1}H and ^{1}H–^{111}Cd.

Lastly, we employed through-space dipolar-based solid-state nuclear magnetic resonance (NMR) methods to experimentally validate the theoretically predicted binding conformation of **1** on the CdS surface. The ^{1}H fast-magic-angle spinning (FMAS) NMR spectra acquired for bare CdS QD gel and one that was exposed to a solution of **1** are shown in **Fig. 5a** and **b**. We observed in the bare gel ^{1}H NMR signals belonging to a trace amount of trioctylphosphine oxide ligands used in the QD synthesis (marked by an asterisk) and signals resonating at 3.6 and 4.7 ppm. The signal at 3.6 ppm originates from the methylene group of

residual thioglycolate ligands from the gel synthesis, while the signal at 4.7 ppm is assigned to physisorbed water or potentially surface S-H groups. Once **1** was added, the signal at 4.7 ppm was removed and replaced by a variety of signals belonging to the adsorbed **1** (**Fig. 5b**, assignments in **Fig. 5f**). The adsorbed **1** was also apparent from a ^{13}C Cross-Polarization Magic-Angle-Spinning (CPMAS) NMR spectrum (**Fig. 5c**) that also displayed a slightly shifted resonance from the thioglycolate carboxyl, suggesting Cd coordination. We performed ^{1}H–^{111}Cd double-echo symmetry-based rotational-echo double-resonance (DE-S-REDOR) experiments to probe the interaction between these species and the CdS surface (**Fig. 5d, e**). (*47, 48*) We only observed dipolar dephasing from the resonances at 4.7 and 3.6 ppm belonging to water and thioglycolate. We fitted these data to a multi-spin model of the CdS surface and found that the water signal is tightly bound to the surface, at only 2.8 Å from the Cd layer. (*47, 49*) Similarly, the thioglycolate CH_2 was closer to the surface than would be expected from bidentate coordination at 3.3 Å from the Cd layer, suggesting the secondary coordination of the thiol.

We additionally performed ^{1}H homonuclear double-quantum correlation experiments (DQ/SQ, **Fig. 5a, b**, bottom) to probe ^{1}H–^{1}H proximities. (*50, 51*) We saw a strong correlation at a double-quantum chemical shift of 10.8 ppm from a proximity between the aromatic ^{1}H's of **1** and the surface-bound thioglycolate. The only logical explanation for this correlation, and the DE-S-REDOR results, is that the CdS surface was partially terminated by thioglycolate ligands, and **1** exists at the surface near these sites. The starkly stronger correlation between these aromatic ^{1}H's and the surface sites, as compared to the alkyl ^{1}H's, nevertheless shows that **1** prefers to adsorb on the surface through its ring structure, in agreement with the theoretical model in **Fig. 4d** and the preferred deuteration observed experimentally in **Fig. 4c**.

In summary, we developed a new heterogeneous photocatalytic hydrogen isotope labeling method for pharmaceuticals. Mechanistic studies revealed a dual HIE pathway mechanism. This unique mechanism unlocked several unique labeling capabilities, including simultaneous labeling of multiple and challenging sites such as secondary α-amino, α-ethereal, allyl, and vinyl sites, providing great versatility in practical uses for pharmaceutical labeling.

ACKNOWLEDGMENTS

Research reported in this publication was primarily supported by the National Science Foundation award number CHE-2247057. R.M. and L.L. are partially funded by the National Institutes of Health award number 1R35 GM142590, the National Science Foundation, Center for Synthetic Organic Electrochemistry, CHE-2002158, the Alfred P. Sloan Foundation (Grant # FH-2023-20829) and the Carl R. Johnson Professorship from Wayne State University. D. L. is funded by the Thomas C. Rumble University Graduate Fellowship from Wayne State University. Solid-state NMR work (FP) was supported by the U.S. Department of Energy, Office of Science, Basic Energy Sciences, Materials Science and Engineering Division, Materials Chemistry. The Ames National Laboratory is operated for the U.S. DOE by Iowa State University under Contract No. DE-AC02-07CH11358. The computational part of this work was supported by the U.S. Department of Energy (DOE), Office of Science, Basic Energy Sciences, under award no. DE-SC0023324, and used resources of the National Energy Research Scientific Computing Center (NERSC), a DOE Office of Science User Facility supported by the Office of Science of the U.S. DOE under contract no. DE-AC02-05CH11231 using NERSC award BES-ERCAP0027306.

Author contributions: Conceptualization: R.M., L.L.; Methodology: R.M., O.D., F.A.P.; Investigation: R.M., O.D., F.A.P., J.L., D.L., S.R., D.L., Z.H., E.M.P., M.A., J.F., T.Q., Z.L., L.L.; Theoretical modeling: M.A., J.F., T.Q., Z.L.; Project administration: J.L., L.L.; Writing-original draft: R.M., L.L.; Writing-review and editing: R.M., O.D., E.M.P., J.L., S.R., Z.L., L.L.

References and Notes

1. C. S. Elmore, The use of isotopically labeled compounds in drug discovery. *Annu. Rep. Med. Chem.* **44**, 515-534 (2009).
2. C. S. Elmore, R. A. Bragg, Isotope chemistry; a useful tool in the drug discovery arsenal. *Bioorg. Med. Chem. Lett.* **25**, 167-171 (2015).
3. J. E. Christian, Radioisotopes in the Pharmaceutical Sciences and Industry. *J. Pharm. Sci.* **50**, 1-13 (1961).
4. A. E. Mutlib, Application of Stable Isotope-Labeled Compounds in Metabolism and in Metabolism-Mediated Toxicity Studies. *Chem. Res. Toxicol.* **21**, 1672-1689 (2008).
5. S. Kopf, F. Bourriquen, W. Li, H. Neumann, K. Junge, M. Beller, Recent Developments for the Deuterium and Tritium Labeling of Organic Molecules. *Chem. Rev.* **122**, 6634-6718 (2022).
6. T. G. Gant, Using deuterium in drug discovery: leaving the label in the drug. *J. Med. Chem.* **57**, 3595-3611 (2014).
7. R. M. C. Di Martino, B. D. Maxwell, T. Pirali, Deuterium in drug discovery: progress, opportunities and challenges. *Nat. Rev. Drug Discov.* **22**, 562-584 (2023).
8. H. Gupta, W. Perkins, C. Stark, S. Kikkeri, J. Kakazu, A. Kaye, A. D. Kaye, Deutetrabenazine for the treatment of chorea associated with Huntington's disease. *Health Psychol. Res.* **10**, (2022).
9. W. J. Kerr, G. J. Knox, L. C. Paterson, Recent advances in iridium(I) catalysis towards directed hydrogen isotope exchange. *J. Labelled Compd. Radiopharm.* **63**, 281-295 (2020).
10. M. Daniel-Bertrand, S. Garcia-Argote, A. Palazzolo, I. Mustieles Marin, P. F. Fazzini, S. Tricard, B. Chaudret, V. Derdau, S. Feuillastre, G. Pieters, Multiple Site Hydrogen Isotope Labelling of Pharmaceuticals. *Angew. Chem. Int. Ed.* **59**, 21114-21120 (2020).
11. W. N. Palmer, P. J. Chirik, Cobalt-Catalyzed Stereoretentive Hydrogen Isotope Exchange of C(sp^3)–H Bonds. *ACS Catal.* **7**, 5674-5678 (2017).
12. H. Yang, C. Zarate, W. N. Palmer, N. Rivera, D. Hesk, P. J. Chirik, Site-Selective Nickel-Catalyzed Hydrogen Isotope Exchange in N-Heterocycles and Its Application to the Tritiation of Pharmaceuticals. *ACS Catal.* **8**, 10210-10218 (2018).
13. R. P. Yu, D. Hesk, N. Rivera, I. Pelczer, P. J. Chirik, Iron-catalysed tritiation of pharmaceuticals. *Nature* **529**, 195-199 (2016).
14. H.-Z. Du, J. Li, S. Christodoulou, S.-Y. Li, Y.-S. Cui, J. Wu, S. Ren, L. Maron, Z.-J. Shi, B.-T. Guan, Directed Aromatic Deuteration and Tritiation of Pharmaceuticals by Heavy Alkali Metal Amide Catalysts. *ACS Catal.* **14**, 9640-9647 (2024).
15. H.-Z. Du, J.-Z. Fan, Z.-Z. Wang, N. A. Strotman, H. Yang, B.-T. Guan, Cesium Amide-Catalyzed Selective Deuteration of Benzylic C-H Bonds with D_2 and Application for Tritiation of Pharmaceuticals. *Angew. Chem. Int. Ed.* **62**, e202214461 (2023).
16. H. Yang, Z. Huang, D. Lehnherr, Y. H. Lam, S. Ren, N. A. Strotman, Efficient Aliphatic Hydrogen-Isotope Exchange with Tritium Gas through the Merger of Photoredox and Hydrogenation Catalysts. *J. Am. Chem. Soc.* **144**, 5010-5022 (2022).

17. Y. Y. Loh, K. Nagao, A. J. Hoover, D. Hesk, N. R. Rivera, S. L. Colletti, I. W. Davies, D. W. MacMillan, Photoredox-catalyzed deuteration and tritiation of pharmaceutical compounds. *Science* **358**, 1182-1187 (2017).
18. Y. Kuang, H. Cao, H. Tang, J. Chew, W. Chen, X. Shi, J. Wu, Visible light driven deuteration of formyl C–H and hydridic C(sp^3)–H bonds in feedstock chemicals and pharmaceutical molecules. *Chem. Sci.* **11**, 8912-8918 (2020).
19. J. Dong, X. Wang, Z. Wang, H. Song, Y. Liu, Q. Wang, Formyl-selective deuteration of aldehydes with D_2O via synergistic organic and photoredox catalysis. *Chem. Sci.* **11**, 1026-1031 (2020).
20. G. Pieters, C. Taglang, E. Bonnefille, T. Gutmann, C. Puente, J.-C. Berthet, C. Dugave, B. Chaudret, B. Rousseau, Regioselective and Stereospecific Deuteration of Bioactive Aza Compounds by the Use of Ruthenium Nanoparticles. *Angew. Chem. Int. Ed.* **53**, 230-234 (2014).
21. Pieters, Enantiospecific C-H activation using ruthenium nanocatalysts. *Angew. Chem. Int. Ed.* **54**, 10474–10477 (2015).
22. E. Levernier, K. Tatoueix, S. Garcia-Argote, V. Pfeifer, R. Kiesling, E. Gravel, S. Feuillastre, G. Pieters, Easy-to-Implement Hydrogen Isotope Exchange for the Labeling of N-Heterocycles, Alkylkamines, Benzylic Scaffolds, and Pharmaceuticals. *JACS Au* **2**, 801-808 (2022).
23. H. Sajiki, N. Ito, H. Esaki, T. Maesawa, T. Maegawa, K. Hirota, Aromatic ring favorable and efficient H–D exchange reaction catalyzed by Pt/C. *Tetrahedron Lett.* **46**, 6995-6998 (2005).
24. N. Behera, D. Gunasekera, J. P. Mahajan, J. Frimpong, Z. F. Liu, L. Luo, Electrochemical hydrogen isotope exchange of amines controlled by alternating current frequency. *Farad. Disc.* **247**, 45-58 (2023).
25. Z. Zhao, R. Zhang, Y. Liu, Z. Zhu, Q. Wang, Y. Qiu, Electrochemical C−H deuteration of pyridine derivatives with D_2O. *Nat. Commun.* **15**, 3832 (2024).
26. L. Shi, M. Liu, L. Zheng, Q. Gao, M. Wang, X. Wang, J. Xiang, Electrochemical γ-Selective Deuteration of Pyridines. *Org. Lett.* **26**, 4318-4322 (2024).
27. G. Prakash, N. Paul, G. A. Oliver, D. B. Werz, D. Maiti, C–H deuteration of organic compounds and potential drug candidates. *Chem. Soc. Rev.* **51**, 3123-3163 (2022).
28. H. Kramp, R. Weck, M. Sandvoss, A. Sib, G. Mencia, P.-F. Fazzini, B. Chaudret, V. Derdau, In situ Generated Iridium Nanoparticles as Hydride Donors in Photoredox-Catalyzed Hydrogen Isotope Exchange Reactions with Deuterium and Tritium Gas. *Angew. Chem. Int. Ed.* **62**, e202308983 (2023).
29. C. C. Hewa-Rahinduwage, X. Geng, K. L. Silva, X. Niu, L. Zhang, S. L. Brock, L. Luo, Reversible Electrochemical Gelation of Metal Chalcogenide Quantum Dots. *J. Am. Chem. Soc.* **142**, 12207-12215 (2020).
30. X. Geng, D. Liu, C. C. Hewa-Rahinduwage, S. L. Brock, L. Luo, Electrochemical Gelation of Metal Chalcogenide Quantum Dots: Applications in Gas Sensing and Photocatalysis. *Acc. Chem. Res.* **56**, 1087-1096 (2023).
31. J. L. Mohanan, I. U. Arachchige, S. L. Brock, Porous semiconductor chalcogenide aerogels. *Science* **307**, 397-400 (2005).
32. D. Liu, A. Hazra, X. Liu, R. Maity, T. Tan, L. Luo, CdS Quantum Dot Gels as a Direct Hydrogen Atom Transfer Photocatalyst for C−H Activation. *Angew. Chem. Int. Ed.*, DOI: e202403186 (2024).

33. C. Huang, J. Qiao, R.-N. Ci, X.-Z. Wang, Y. Wang, J.-H. Wang, B. Chen, C.-H. Tung, L.-Z. Wu, Quantum dots enable direct alkylation and arylation of allylic C(sp^3)–H bonds with hydrogen evolution by solar energy. *Chem* **7**, 1244-1257 (2021).
34. Y. Jiang, C. Wang, C. R. Rogers, M. S. Kodaimati, E. A. Weiss, Regio-and diastereoselective intermolecular [2+ 2] cycloadditions photocatalysed by quantum dots. *Nat. Chem.* **11**, 1034-1040 (2019).
35. Y. Jiang, R. López-Arteaga, E. A. Weiss, Quantum dots photocatalyze intermolecular [2+ 2] cycloadditions of aromatic alkenes adsorbed to their surfaces via van der Waals interactions. *J. Am. Chem. Soc.* **144**, 3782-3786 (2022).
36. Y. R. Luo, *Handbook of Bond Dissociation Energies in Organic Compounds*. (CRC Press, 2002).
37. W. Cao, A. Yakimov, X. Qian, J. Li, X. Peng, X. Kong, C. Copéret, Surface Sites and Ligation in Amine-capped CdSe Nanocrystals. *Angew. Chem. Int. Ed.* **62**, e202312713 (2023).
38. C. Huang, R.-N. Ci, J. Qiao, X.-Z. Wang, K. Feng, B. Chen, C.-H. Tung, L.-Z. Wu, Direct Allylic C(sp^3)−H and Vinylic C(sp^2)−H Thiolation with Hydrogen Evolution by Quantum Dots and Visible Light. *Angew. Chem. Int. Ed.* **60**, 11779-11783 (2021).
39. G. E. Dobereiner, R. H. Crabtree, Dehydrogenation as a Substrate-Activating Strategy in Homogeneous Transition-Metal Catalysis. *Chem. Rev.* **110**, 681-703 (2010).
40. L. Neubert, D. Michalik, S. Bähn, S. Imm, H. Neumann, J. Atzrodt, V. Derdau, W. Holla, M. Beller, Ruthenium-Catalyzed Selective α,β-Deuteration of Bioactive Amines. *J. Am. Chem. Soc.* **134**, 12239-12244 (2012).
41. B. Chatterjee, V. Krishnakumar, C. Gunanathan, Selective α-Deuteration of Amines and Amino Acids Using D_2O. *Org. Lett.* **18**, 5892-5895 (2016).
42. M. Takahashi, K. Oshima, S. Matsubara, Ruthenium Catalyzed Deuterium Labelling of α-Carbon in Primary Alcohol and Primary/Secondary Amine in D_2O. *Chem. Lett.* **34**, 192-193 (2005).
43. D. Hesk, S. Borges, S. Hendershot, D. Koharski, P. McNamara, S. Ren, S. Saluja, V. Truong, K. Voronin, Synthesis of ^3H, $^2H_4$ and ^{14} C-SCH 417690 (Vicriviroc). *J. Labelled Comp. Radiopharm.* **59**, 190-196 (2016).
44. K. J. Wu, D. Klepacki, A. S. Mankin, A. G. Myers, A method for tritiation of iboxamycin permits measurement of its ribosomal binding. *Bioorg. Med. Chem. Lett.* **91**, 129364 (2023).
45. D. Hesk, S. Borges, R. Dumpit, S. Hendershot, D. Koharski, P. McNamara, S. Ren, S. Saluja, V. Truong, K. Voronin, Synthesis of ^3H, $^2H_4$, and ^{14}C - MK 3814 (preladenant). *J. Labelled Compd. Radiopharm.* **60**, 194-199 (2017).
46. R. I. Cukier, A Theory that Connects Proton-Coupled Electron-Transfer and Hydrogen-Atom Transfer Reactions. *J. Phys. Chem. B* **106**, 1746-1757 (2002).
47. L. Chen, Q. Wang, B. Hu, O. Lafon, J. Trébosc, F. Deng, J.-P. Amoureux, Measurement of hetero-nuclear distances using a symmetry-based pulse sequence in solid-state NMR. *Phys. Chem. Chem. Phys.* **12**, 9395-9405 (2010).
48. B. A. Atterberry, S. L. Carnahan, Y. Chen, A. Venkatesh, A. J. Rossini, Double echo symmetry-based REDOR and RESPDOR pulse sequences for proton detected measurements of heteronuclear dipolar coupling constants. *J Magn Reson Open* **336**, 107147 (2022).
49. J. Cunningham, F. A. Perras, INTERFACES. A program for determining the 3D structures of surfaces sites using NMR data. *J Magn Reson Open* **12-13**, 100066 (2022).

50. Y. Nishiyama, V. Agarwal, R. Zhang, Efficient symmetry-based γ-encoded DQ recoupling sequences for suppression of t1-noise in solid-state NMR spectroscopy at fast MAS. *Solid State Nucl. Magn. Reson.* **114**, 101734 (2021).
51. M. Feike, D. E. Demco, R. Graf, J. Gottwald, S. Hafner, H. W. Spiess, Broadband Multiple-Quantum NMR Spectroscopy. *J Magn Reson Open* **122**, 214-221 (1996).